J Mater Sci (2010) 45:6446–6454
DOI 10.1007/s10853-010-4730-y

Tensile impact behavior and deformation mechanism of duplex TiAl intermetallics at elevated temperatures

Xiang Zan · Yuehui He · Yang Wang · Zhengxin Lu · Yuanming Xia

Received: 7 January 2010 / Accepted: 18 June 2010 / Published online: 1 July 2010

Abstract Investigations are made on the effects of strain rates on the tensile behavior and deformation modes of Duplex Ti–46.5Al–2Nb–2Cr (DP TiAl) at temperatures ranging from room temperature to 840 °C and under strain rates of 0.001, 320, 800, and 1350 s^{-1}. The dynamic strength is higher than quasi-static strength but does not change much over the high strain rate range. Yield stress anomaly is not found. Brittle-to-ductile transition temperature (BDTT) increases with the increased strain rates. A Zerilli–Armstrong constitutive model with appropriate coefficients is chosen to describe the high strain rate flowing behavior. TEM analysis indicates that both ordinary dislocations and superdislocations are found and dislocation pile-up only appears in samples deformed under quasi-static loadings at elevated temperatures. The deformation twins are common in equiaxed grains and the proportion of twinned grains increases with the increased strain rate from 46–72% under quasi-static loadings to 69–95% under high strain rate loadings. No deformation twins are found in lamellar colonies.

X. Zan (✉) · Y. Wang · Y. Xia
Department of Modern Mechanics, CAS Key Laboratory of Mechanical Behavior and Design of Materials, University of Science and Technology of China, 230027 Hefei, People's Republic of China
e-mail: zanx@ustc.edu.cn

Y. He
State Key Laboratory for Powder Metallurgy, Central South University, 410083 Changsha, People's Republic of China

Z. Lu
School of Materials Science and Technology, Advanced Material Analysis and Test Center, Xi'an University of Technology, 710048 Xi'an, People's Republic of China

Introduction

γ-TiAl is of the face-centered tetragonal (FCT) crystal structure with lattice parameters of $c/a = 1.02$. Although the FCT structure appears similar to the face-centered cubic (FCC) structure, because of long range ordered superlattice and lower crystal symmetry, the number of independent slip system in the former is far smaller than that in the latter [1, 2]. The superlattice structure of TiAl reduces dislocation mobility and results in lower ductility and fracture toughness [3]. Abundant researches indicate that the primary modes of deformation for γ-TiAl under quasi-static loadings at different temperatures are $\langle 110]$ ordinary slip, $\langle 101]$ superdislocation, and $1/6\langle 11\bar{2}]\{111\}$ twinning [2, 3]. However, the aforementioned deformation mechanism does not change TiAl crystal lattice and the TiAl superlattice can be kept near the melt point [4]. So TiAl shows its potentially attractive properties for high-temperature structural applications, properties such as low density, good oxidation, and burn resistance and high-temperature strength retention [2, 3, 5–8].

A wealth of literature describes its mechanical behavior, composition, and microstructures [2, 3, 8–15]. Kim [2, 5, 7] and Appel [3] also reviewed in detail the deformation and mechanical behavior of TiAl.

Some literature on mechanical behavior of TiAl under dynamic or high strain rate loadings has been reported. Gray [6, 16] of Los Alamos National Laboratory, cooperating with Maloy and Gray [17], Jin et al. [18–20], Vaidya et al. [21], Mckenna et al. [22], Cerreta et al. [23] and Millett et al. [24], investigated the dynamic behavior of TiAl with different methods such as dynamic compression, high speed particle impact, Taylor cylinder impact, and shock loadings, respectively. Shazly et al. [25] also investigated the uniaxial mechanical behavior under

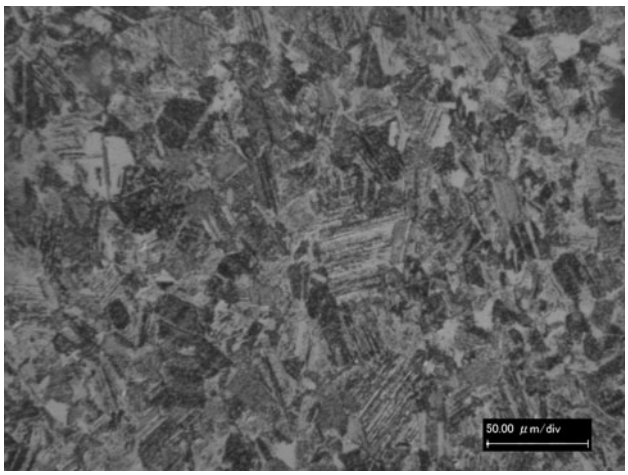

Fig. 1 Optical micrograph of DP Ti–46.5–Al2Nb–2Cr (×1000)

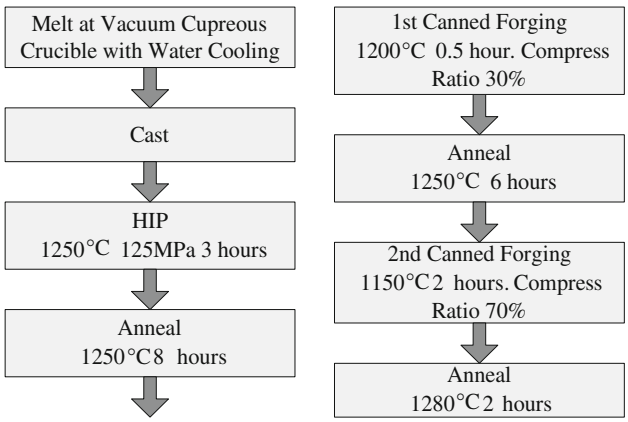

Fig. 2 Diagram of material preparing process

compression of Gamma-Met PX and Ti–45Al–X(Nb, B, C) with nearly lamellar microstructures, at elevated temperatures and high strain rates. These investigations show that the mechanical behavior of TiAl under dynamic loadings is different from that under quasi-static loadings. However, many materials show different mechanical behaviors under tensile and compressive loadings. The γ-TiAl can be

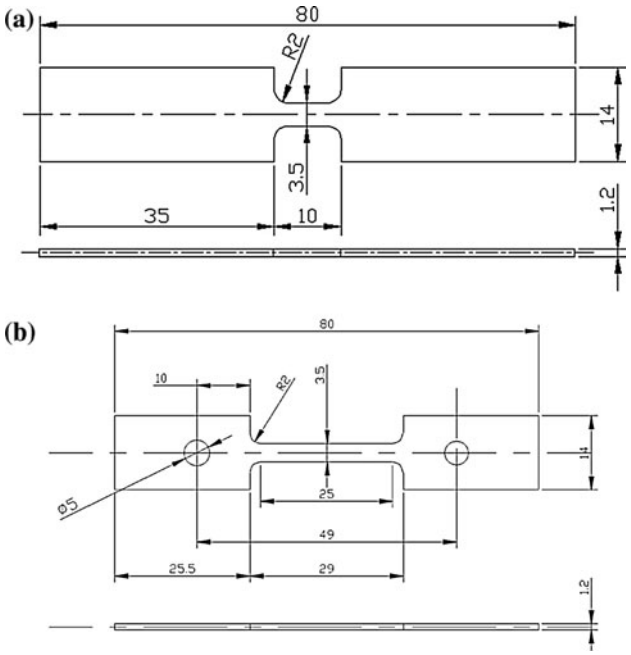

Fig. 4 Diagrams of specimens used in **a** tensile impact and **b** quasi-static experiments

deformed under compression at room temperature and strains of 8%, with no occurrence of cracking, whereas nearly zero ductility results under tensile loadings [4]. So it is necessary to investigate the dynamic tensile behavior of TiAl in order to systematically study the mechanical behavior of these alloys at various strain rates so as to satisfy the conditions required in the proposed applications of TiAl to jet turbines and other propulsion system components [21].

A few papers have reported the dynamic tensile behavior of TiAl. Wang, Lin, and Zhou [26–28] studied the dynamic tensile behavior of Ti–47Al–X(Mn, Nb, Cr) with a lamellar microstructure at room temperatures and found that the dynamic strength is higher than that under quasi-static loadings, revealing different strain rate sensitivities within different strain rate ranges. Sun et al. [29]

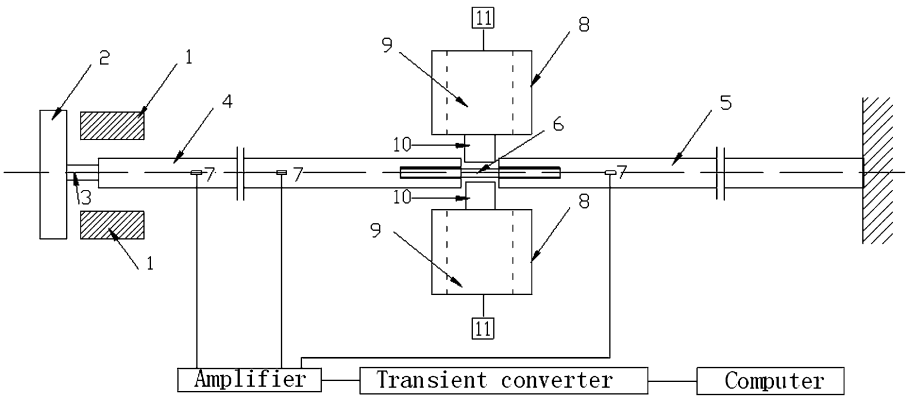

Fig. 3 Schematic diagram of split Hopkinson tension bar (BTIA at USTC) with rapid heating system. *1* Impact hammer, *2* impact block, *3* short metal bar, *4* input bar, *5* output bar, *6* specimen, *7* strain gauge, *8* furnaces, *9* heat storages, *10* copper conductors, *11* thermocouples

investigated the deformation mechanism of duplex Ti–45Al–1.6Mn at the maximum strain rate of 300 s^{-1} and found that dislocation and twinning mechanisms change with increased strain rates. But his work was also done at room temperature (RT). For a structural material used at elevated temperatures, its data collected only at RT are not sufficient. Shazly et al. [25] reported tensile impact behavior of Gamma-Met PX at elevated temperatures up to 900 °C. But the report gave only the stress–strain curves and SEM micrographs of the fracture surfaces.

The purpose of this article is to analyze the effects of strain rates (0.001–1350 s^{-1}) on the tensile mechanical and deformation modes of duplex Ti–46.5Al–2Nb–2Cr (DP TiAl) within a wide range of temperatures (RT to 840 °C).

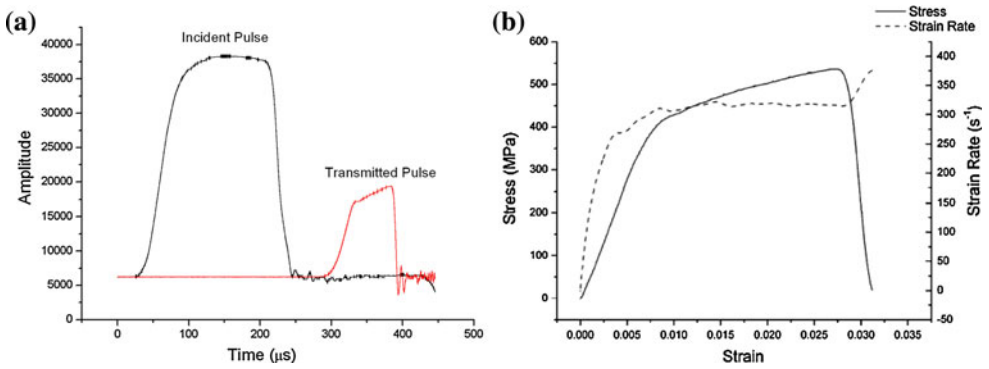

Fig. 5 Typical **a** incident and transmitted pulse and **b** the $\sigma - \varepsilon$ and $\dot{\varepsilon} - \varepsilon$ curves

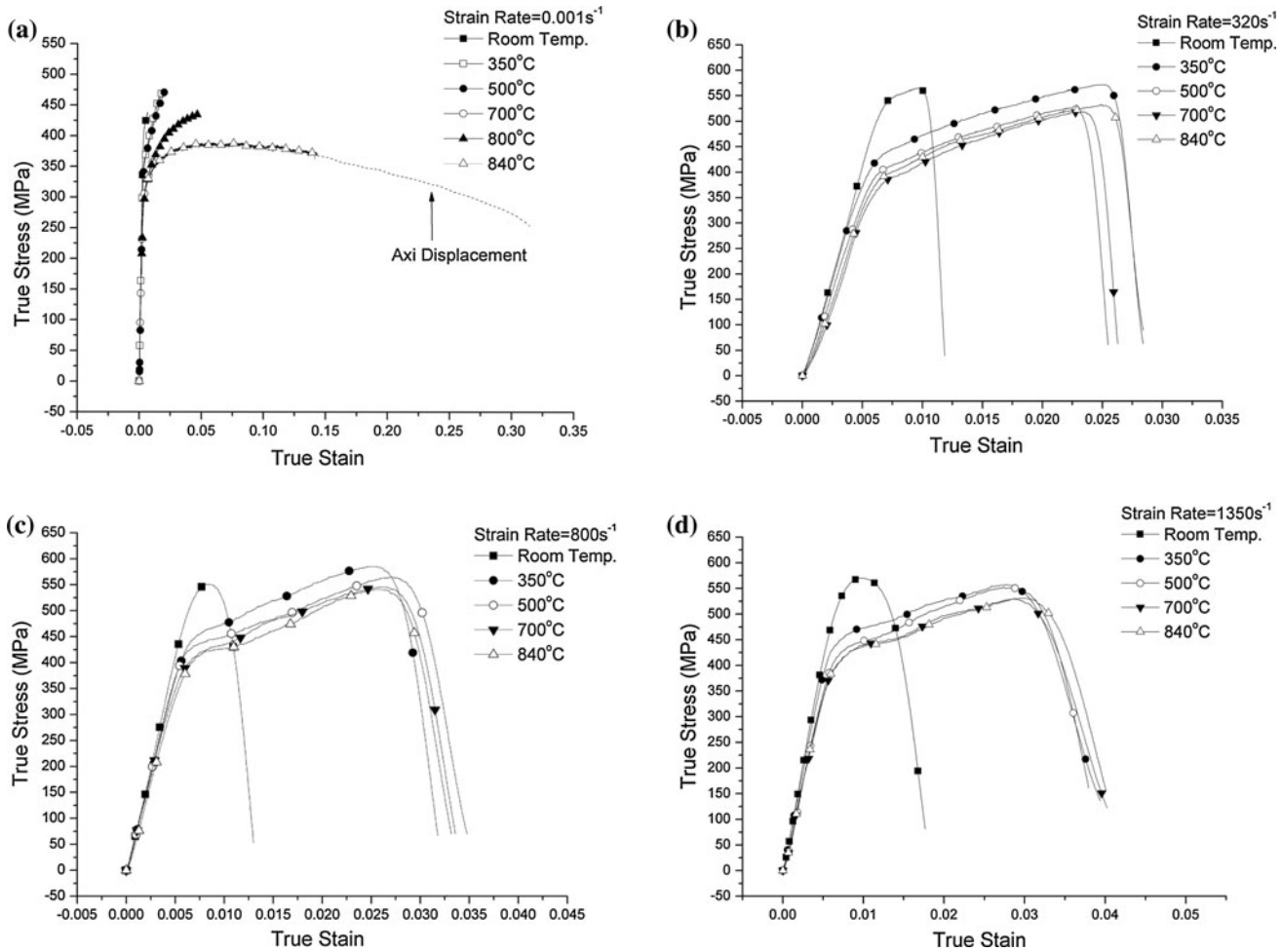

Fig. 6 True stress–true strain curves at strain rates of **a** 0.001, **b** 320, **c** 800, and **d** 1350 s^{-1}

Materials and experimental procedure

The microstructure of DP TiAl shown in Fig. 1 is prepared as diagrammed in Fig. 2. The can materials in canned forging process is 45# steel (Chinese model), and the fill material is aluminum oxide powder.

The tensile impact behaviors of DP TiAl under strain rates of 320, 800, and 1350 s^{-1} at temperatures ranging from RT to 840 °C is carried out on the Rotating Disk Indirect Bar–Bar Tensile Impact Apparatus (BTIA) at USTC, a type of split Hopkinson tensile bar (SHTB), using a rapid contact heating technique (Fig. 3) [30–33]. The width and amplitude of input pulses can be easily controlled by the "short metal bar" (part 3 in Fig. 3) [30]. Corresponding quasi-static tests at a strain rate of 0.001 s^{-1} are achieved on MTS 809. Figure 4 shows the diagrams of electro-discharge machined specimens used in (a) tensile impact and (b) quasi-static experiments, respectively. Detailed experimental process can be found elsewhere [34, 35].

For transmission electron microscope (TEM) analysis, samples are taken parallel to the loading axis from broken specimens and then sliced, ground and polished to 80–100 μm-thick foils, out of which are punched 3 mm disks. Afterwards, the disks are twinjet polished with a solution (methanol:butanol:perchloric acid = 60:35:5) until holes appear. The TEM disks are examined with a JEOL JEM 3010 operating at 300 kV.

Experimental results and discussions

Mechanical behavior

In tensile impact tests, the incident pulse is smooth and stable without oscillations (Fig. 5a) and the signal recording system is able to record the rising stage of the pulse [30]. Figure 6 shows the true strain–true stress curves of DP TiAl at different strain rates and Fig. 7 the temperature and strain rate effects of yield stress $\sigma_{0.2}$ (0.2% proof

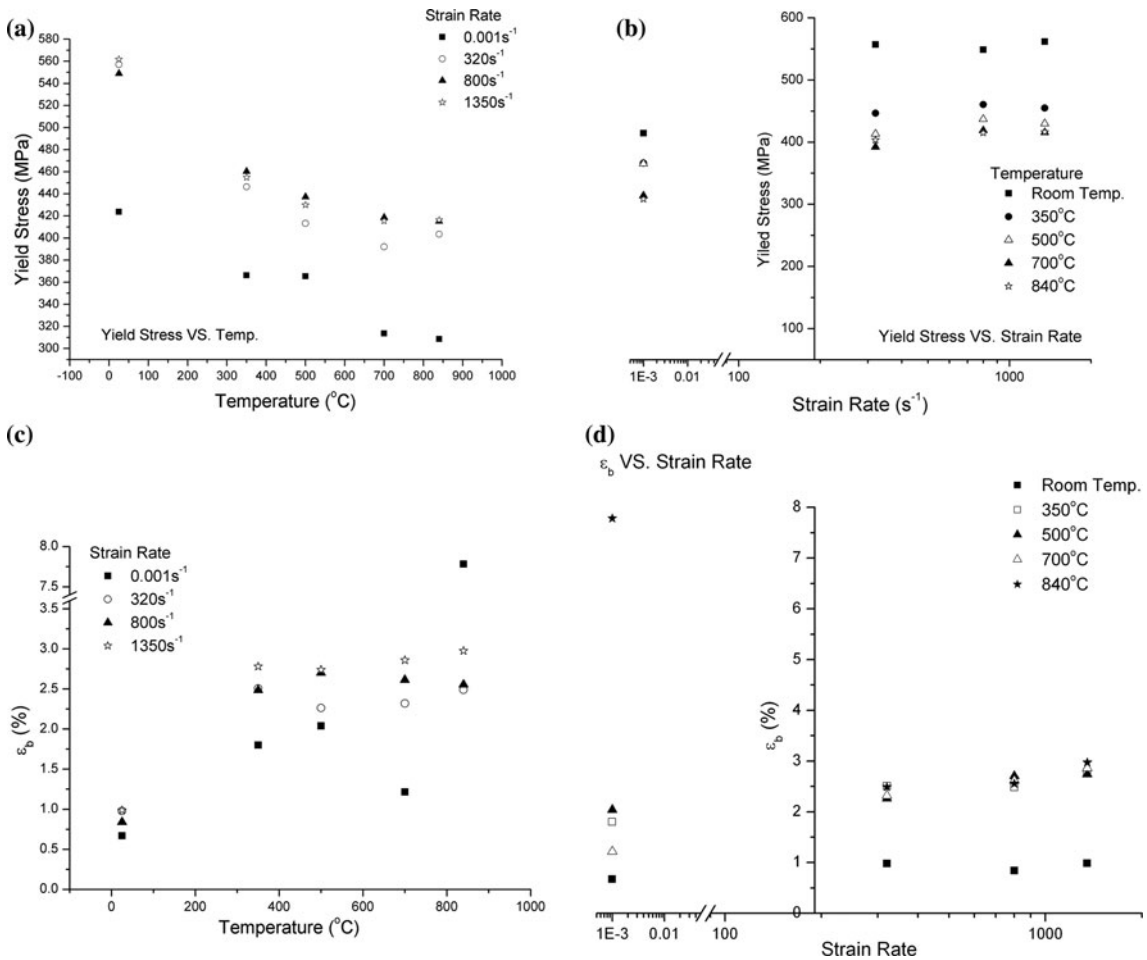

Fig. 7 Temperature and strain rate effects of yield stress and unstable strain of DP TiAl

stress) and unstable strain ε_b (strain corresponding to the ultimate tensile strength (UTS)). By comparing the $\sigma - \varepsilon$ and $\dot{\varepsilon} - \varepsilon$ curves (Fig. 5b), it could be found that the strain rate curve has already reached a stable stage before the material yields. So, the value of $\sigma_{0.2}$ is acceptable. Here, $\sigma_{0.2}$ is the average of the values at the yield points in several true stress–true strain curves under the same loading conditions and ε_b is the same.

From Figs. 6 and 7, it can be concluded that (1) Dynamic strengths including $\sigma_{0.2}$, UTS and flowing stress corresponding to the same strain are higher than those under quasi-static loadings at the same temperature but, within the high strain rate range (320–1350 s^{-1}), dynamic strengths are nearly strain rate independent; (2) No yield stress anomaly is found; (3) At 840 °C, brittle-to-ductile transition (BDT) occurs under quasi-static loadings whereas the whole deformation remains less than 4% under high strain rate loadings—that is to say, the brittle-to-ductile transition temperature (BDTT) increases with increased strain rates; (4) Below BDTT, unstable strain ε_b under dynamic loadings is slightly larger than that under quasi-static loadings; (5) Below BDTT, the strain-hardening/work-hardening rate ($d\sigma/d\varepsilon$) attains around 6000 MPa/unit strain under quasi-static loadings and slightly increases to about 6500 MPa/unit strain under high strain rate loadings; (6) From 350 to 840 °C, the work-hardening rate under high strain rate loadings is not sensitive to the temperatures and strain rates. Details of temperature and strain rate effects of other parameters and fracture modes can be found elsewhere [34, 35].

Constitutive equations

Constitutive equations play an important role in deformation simulation. The current study employs the Zerilli–Armstrong (Z–A) model [36, 37], based on dislocation movement mechanics, to describe the dynamic mechanical behavior of DP TiAl. The Z–A models corresponding to the two most common crystal structures, FCC and BCC (body-center cubic), are given as follows:

$$\sigma = C_0 + C_2\varepsilon^{1/2}\exp\left(-C_3T + C_4T\ln\frac{\dot{\varepsilon}}{\dot{\varepsilon}_0}\right) \quad \text{(FCC)} \qquad (1)$$

$$\sigma = C_0 + C_1\exp\left(-C_3T + C_4T\ln\frac{\dot{\varepsilon}}{\dot{\varepsilon}_0}\right) + C_5\varepsilon^n \quad \text{(BCC)} \qquad (2)$$

in which C_0 is the thermal component of stress containing the grain size effect, C_1 the coefficient of the thermal stress term, C_2 and C_3 the thermal softening coefficients, C_4 the coefficient of the temperature and strain rate coupling term, $\dot{\varepsilon}_0 = 1\ s^{-1}$ the reference strain rate and C_5 and n are the work-hardening coefficient and exponent, respectively.

Table 1 Coefficients of Zerilli–Armstrong constitutive BCC model of DP TiAl

	C_0 (MPa)	C_1 (MPa)	C_3 (K^{-1})	C_4 (K^{-1})	C_5 (MPa)	n
DP TiAl	391	371	6.99E−4	−5.64E−4	2.71E3	0.750

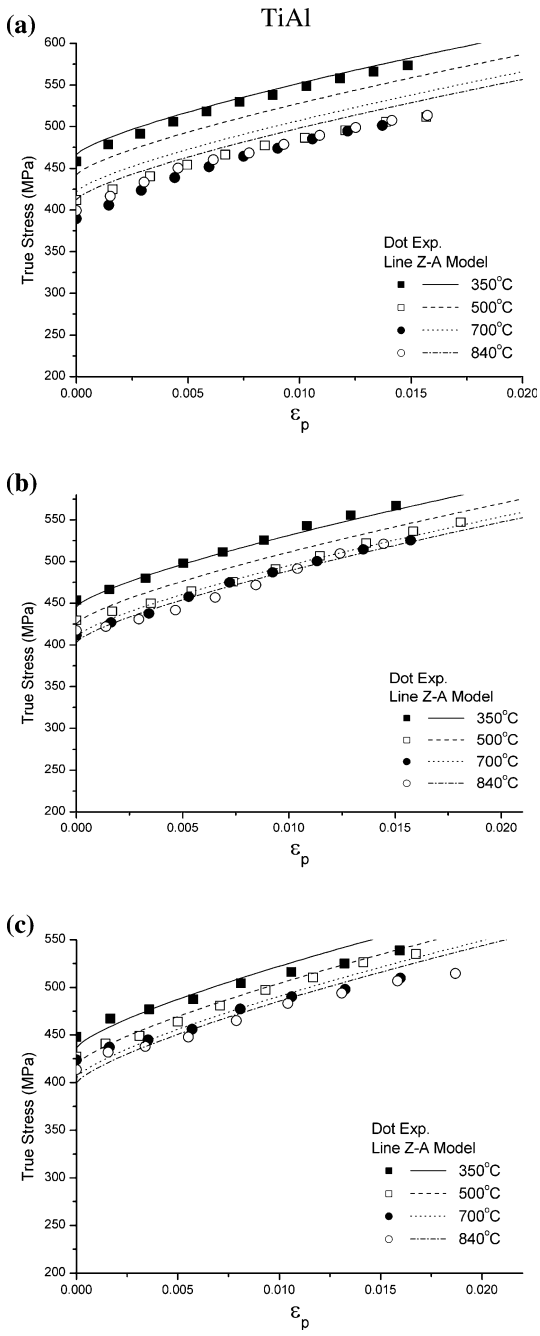

Fig. 8 Comparison between measured and calculated stress–strain curves at different temperatures and strain rates. **a** 320 s^{-1}, **b** 800 s^{-1}, **c** 1350 s^{-1}

In Eq. 1, the work-hardening rate is temperature and strain rate dependent. On the contrary, in Eq. 2, it is temperature and strain rate independent. In "Mechanical behavior" section, it is pointed out that, from 350 to 840 °C, the work-hardening rate under high strain rate loadings is not sensitive to the temperatures and strain rates. In addition, although TiAl FCT structure appears similar to FCC structure, the deformation modes of TiAl are not the same as those of FCC metals, because of its limited independent slip system. Deformation twinning is the main deformation mode in TiAl, which is common in BCC metals. Therefore, in this study, Eq. 2, i.e., the BCC model, is chosen to describe the dynamic flowing behavior of DP TiAl under high strain rate loadings.

Generally, under high strain rate loadings, the heat generation during the adiabatic deformation process is not neglectable. Since the total plastic deformation of DP TiAl in this study is only less than 3%, the adiabatic temperature rising is not taken into consideration. Consequently in Z–A BCC model, T is the experimental temperature applied. Table 1 presents the coefficients of the constitutive equation obtained for DP TiAl. Figure 8 compares the experimental and calculated curves. The results show that Z–A BCC model performs well in describing the dynamic flowing behavior of DP TiAl at elevated temperatures.

Microstructure

In Fig. 1, large annealing twins can be seen in equiaxed γ grains, hence no need for their detailed TEM images. Discussion is made about the temperature and strain rate effects on microstructure evaluation of DP TiAl.

Figures 9, 10, 11 and 12, 13, 14 show the TEM micrographs of the equiaxed grain of DP TiAl after quasi-static and high strain rate tensile tests at different temperatures, respectively. Deformation twins are quite common. Observations under different reflection conditions may result in different contrasts of the deformation twins.

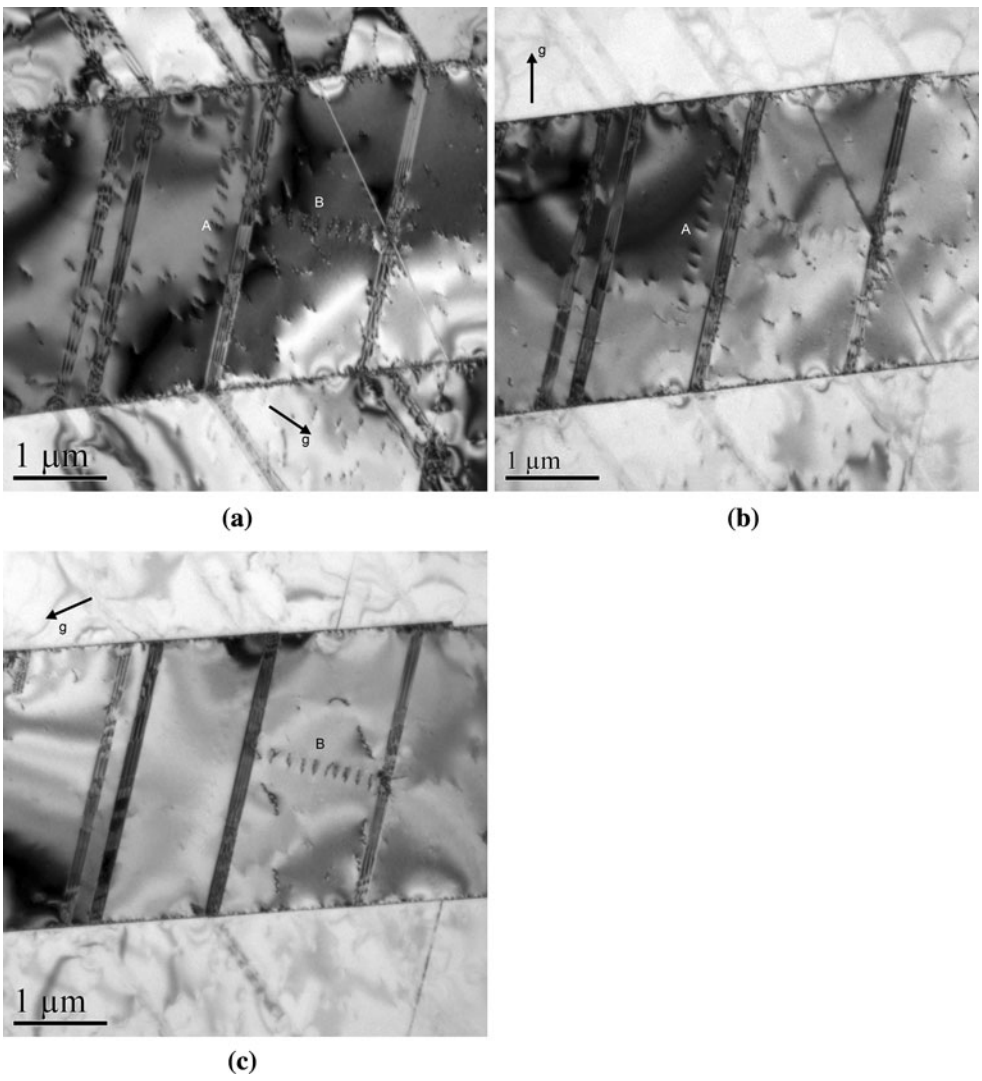

Fig. 9 The microstructure after deformation at RT and quasi-static loading with different **g** (ZONE = [110]). **a** **g** = 002, **b** **g** = $1\bar{1}\bar{1}$, **c** **g** = $\bar{1}1\bar{1}$

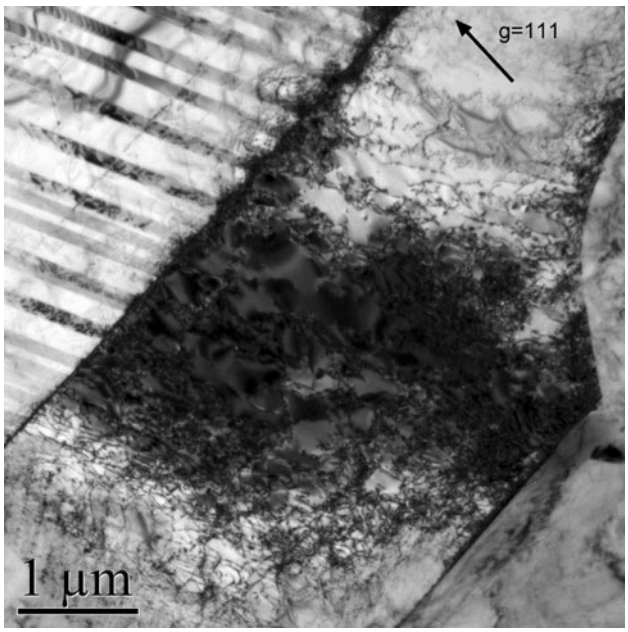

Fig. 10 The microstructure after deformation at 500 °C and quasi-static loading ($\mathbf{g} = 111$)

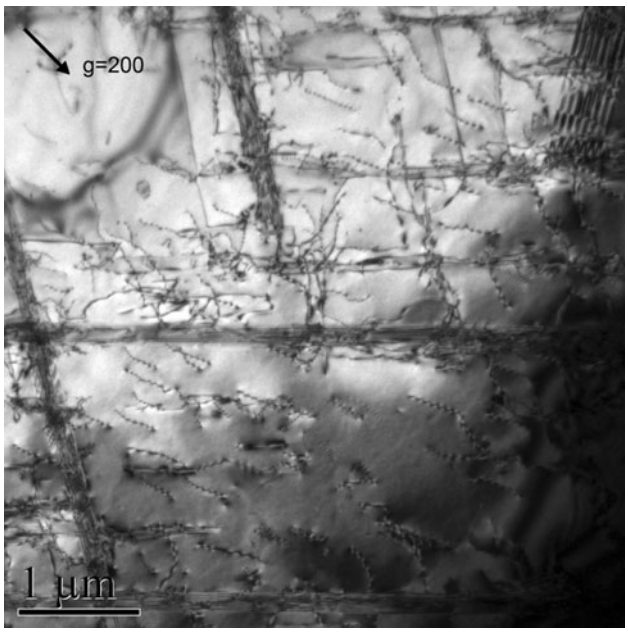

Fig. 12 The microstructure of DP TiAl after deformation at RT and strain rate of 1350 s^{-1}

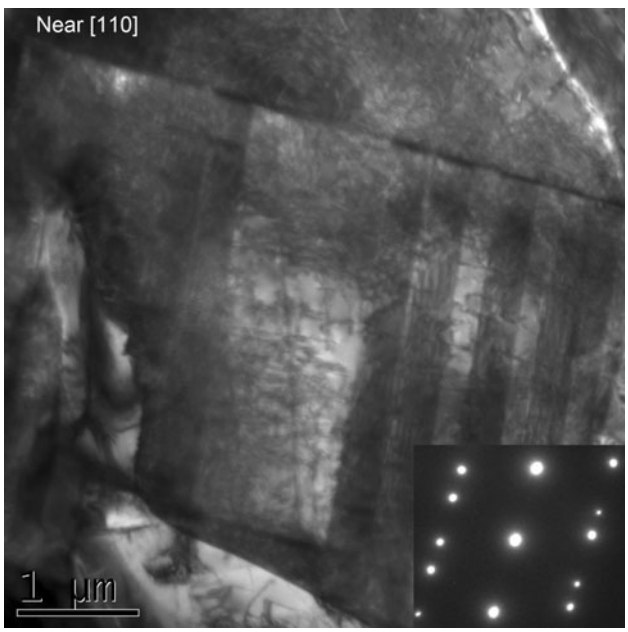

Fig. 11 The microstructure after deformation at 700 °C and quasi-static loading

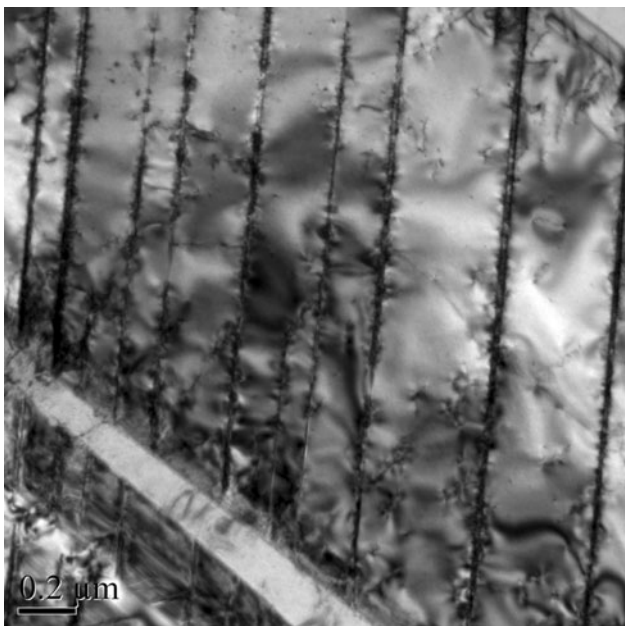

Fig. 13 The microstructure of DP TiAl after deformation at 350 °C and strain rate of 320 s^{-1} (ZONE = [110])

Deformation twins originate at the grain boundary and propagate on multiple {111} slip planes through the primary γ grains. Most of the twins can easily propagate across the annealing twin boundaries (Figs. 9, 13, 14). In some grains, twins on different {111} planes intersect each other, most terminating at the grain boundary and a few inside the grain (the left of Fig. 9c and the up-right of Fig. 12).

In order to understand the dislocation slip behavior of the material, the Burgers vector analysis is conducted using the general invisibility condition $\mathbf{g} \cdot \mathbf{b} = 0$ to identify the dislocation features in the γ phase [29, 38]. Figure 9

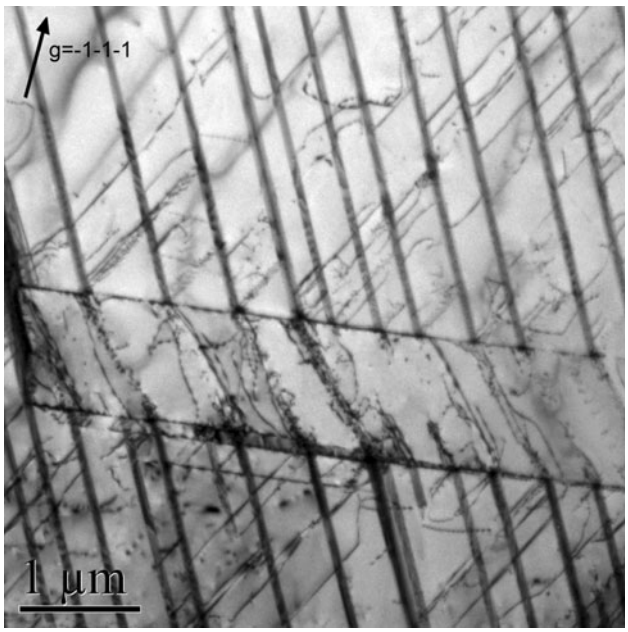

Fig. 14 The microstructure of DP TiAl after deformation at 840 °C and strain rate of 1350 s^{-1}

exhibits the TEM images of the same location in an equiaxed γ grain with different operative reflections. It can be seen that A and B are both visible under reflection of $\mathbf{g} = 002$. However, only dislocations in direction A are visible under $\mathbf{g} = 1\bar{1}\bar{1}$ and only dislocations in direction B under $\mathbf{g} = \bar{1}1\bar{1}$. Thereupon, dislocations in directions A and B are all superdislocations with different Burgers vectors of $\mathbf{b} = [10\bar{1}]$ and $\mathbf{b} = [101]$, respectively. It is very interesting that the dislocations in direction A or B are parallel to each other and of about the same length. In addition, the long axes of these arrays of dislocations are either parallel (A) or perpendicular (B) to the twin fringe. ⟨110] ordinary dislocations are also found in some grains. Moreover, dislocation pile-up appears after deformation at elevated temperatures (Fig. 11), but does not in samples deformed under high strain rate loadings.

Figure 15 shows the deformation microstructure of lamellar colonies deformed at different temperatures and strain rates. In no case do deformation twins appear, but dislocations are found after deformation at elevated temperatures (Fig. 15b).

Different grains are of different orientations. Owing to their sensitivity to the loading direction, the microstructure of each grain may evolve differently. Of the equiaxed grains, some are twinned while the others are deformed only by dislocation (the middle of Fig. 10). The number of twins and the space between the twins in each grain are irregular, but the proportion of twinned grains can be accounted for. With the increased temperatures (RT ~840 °C), 46–72% of the grains are twinned under quasi-static loadings, whereas the proportion increases to 69–95% under high strain rate loadings.

In TiAl, as the strain rate increases, resistance to dislocation motion increases and the grains tend to twin, due to the fact that the value of the Burgerous vector for twinning is less than that for superdislocation [38, 39]. Additionally, twin-growth rate can reach nearly sound speed, while dislocation movement velocity is much lower [40]. Under high strain rate loadings, the fracture strain is less than 4% and the whole deformation time is less than 100 μs. During this extremely short period of time, deformation twins grow more easily and hence more twinned grains.

The proportion of the twinned grains of samples deformed over the temperature range of 350–840 °C under high strain rate loadings keeps about 89–95%. As mentioned above, dislocation pile-up is not found in those samples. It is possible to be of the opinion that twinning is the main deformation mode of DP TiAl under high strain

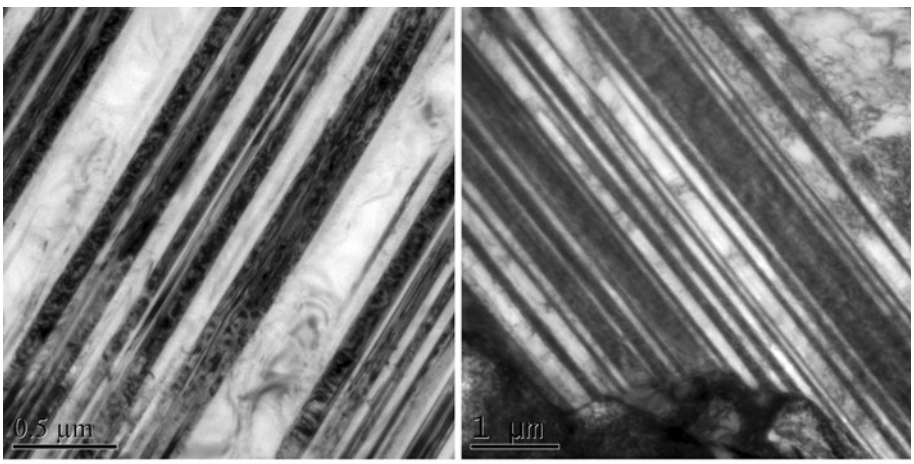

Fig. 15 Lamellar colonies of DP TiAl after deformation (beam direction near **a** [110] and **b** [112])

rate loadings and at elevated temperatures. It is well known that dislocation motion is highly sensitive to strain rate and temperature, while twinning has a much lower sensitivity [41, 42]. Hence the low sensitivity of the high-temperature dynamic behavior of DP TiAl.

Summary

In this study, mechanical behavior and deformation mechanism of duplex Ti–46.5Al–2Nb–2Cr at different temperatures and strain rates are investigated. The test results show that (1) Dynamic strength is higher than that under quasi-static loadings but, over the high strain rate range (320–1350 s^{-1}), almost no strain rate effects occur; (2) No yield stress anomaly is found and BDTT increases with the increased strain rates; (3) Below BDTT, the work-hardening rate ($d\sigma/d\varepsilon$) attains around 6000 MPa/unit strain under quasi-static loadings and slightly increases to about 6500 MPa/unit strain under high strain rate loadings; (4) From 350 to 840 °C, the work-hardening rate under high strain rate loadings is not sensitive to temperature and strain rate.

TEM investigations show that (1) Both ordinary dislocations and superdislocations are found in DP TiAl after deformation under different loading conditions and dislocation pile-up appears only in samples deformed under quasi-static loadings at elevated temperatures; (2) No deformation twins are found in grains of lamellar colonies while those are common in equiaxed grains; (3) The proportion of twinned equiaxed grains increase with the increased strain rate from 46–72% under quasi-static loadings to 69–95% under high strain rate loadings.

Acknowledgements The authors are very grateful to Mr. Yuzhang Chen and Dr. Yao Jiang of State Key Laboratory for Powder Metallurgy, Central South University, for the materials preparation and Xuhui Gong, Zhonglin Duan, and Xinzhong Ma for their help in the experiments. This project is supported by the National Natural Science Foundation of China (Project No.: 10902106 and 90505002).

References

1. Marketz WT, Fischer FD, Clemens H (2003) Int J Plast 19:281
2. Kim Y-W (1994) JOM 46:30
3. Appel F, Wagner R (1998) Mater Sci Eng R Rep 22:187
4. Shechtman D, Blackburn M, Lipsitt H (1974) Metall Trans 5:1373
5. Kim Y-W (1989) JOM 41:24
6. Gray GT III (1991) In: Microstructure/property relationships in titanium aluminides and alloys. TMS, Detroit
7. Kim Y-W, Dimiduk DM (1991) JOM 43:41
8. Clemens H, Kestler H (2000) Adv Eng Mater 2:551
9. Huang SC, Chesnutt JC (2000) In: Westbrook JH, Fleischer RL (eds) Intermetallic compounds, volume 3—structural applications of intermetallic compounds. Wiley, New York
10. Yamaguchi M, Inui H, Ito K (2000) Acta Mater 48:307
11. Liu CT, Stringer J, Mundy JN, Horton LL, Angelini P (1997) Intermetallics 5:579
12. Liu CT (1995) Mater Chem Phys 42:77
13. Appel F, Brossmann U, Christoph U, Eggert S, Janschek P, Lorenz U, Müllauer J, Oehring M, Paul JDH (2000) Adv Eng Mater 2:699
14. Yamaguchi M, Inui H, Yokoshima S, Kishida K, Johnson DR (1996) Mater Sci Eng A 213:25
15. Kumpfert J, Kim YW, Dimiduk DM (1995) Mater Sci Eng A 192–193:465
16. Gray GT III (1993) Deformation twinning: influence of strain rate. Pittsburgh, PA
17. Maloy SA, Gray GT III (1996) Acta Mater 44:1741
18. Jin Z, Cady C, Gray GT III, Kim YW (1996) In: Soboyejo WO, Srivatsan TS, Fraser HL (eds) Deformation and fracture of ordered intermetallic materials III. TMS, Cincinnati
19. Jin Z, Cady C, Gray GT III, Kim Y-W (2000) Metall Mater Trans A 31:1007
20. Jin Z, Gray GT, Yamaguchi M (1996) In: Koch CC, Liu CT, Stoloff NS, Wanner A (eds) Symposium on high-temperature ordered intermetallic alloys VII. Materials Research Society, Boston, MA, p 189
21. Vaidya RU, Jin Z, Cady C, Gray GT III, Butt DP (1999) Scr Mater 41:569
22. McKenna V, Rubal M, Steif P, Pereira J, Gray G (2002) Metall Mater Trans A 33:581
23. Cerreta E, Chen S, Gray G, Pollock T (2004) Metall Mater Trans A 35:2557
24. Millett J, Gray GT, Bourne N (2000) J Appl Phys 88:3290
25. Shazly M, Prakash V, Draper S (2004) Int J Solids Struct 41:6485
26. Wang Y, Lin D, Zhou Y, Xia Y, Law CC (1999) J Mater Sci 34:509. doi:10.1023/A:1004538511115
27. Wang Y, Lin D, Kim Y-W (1999) Trans Nonferrous Met Soc China 9:437
28. Zhou Y, Xia Y (2000) J Mater Sci 35:925. doi:10.1023/A:1004754525806
29. Sun ZM, Kobayashi T, Fukumasu H, Yamamoto I, Shibue K (1998) Metall Mater Trans A 29:263
30. Xia YM, Wang Y (2007) J Test Eval 35:1
31. Zan X, Chen X, Huang W, Xia Y (2005) J Exp Mech 20:321
32. Huang W, Zan X, Nie X, Gong M, Wang Y, Xia YM (2007) Mater Sci Eng A 443:33
33. Huang W, Zan X, Huang S, Wang Y, Xia Y (2005) In: SAE 2005 World Congress & Exhibition
34. Zan X, Wang Y, Xia Y, He Y (2008) Mater Sci Eng A 498:296
35. Zan X, Duan ZL, Wang Y, Xia YM, He YH (2008) In: Kim YW, Morris D, Yang R, Leyens C (eds) Structural aluminides for elevated temperatures: gamma titanium and other: metallic aluminides. The Minerals, Metals & Materials Society, Warrendale
36. Zerilli FJ, Armstrong RW (1987) J Appl Phys 61:1816
37. Johnson GR, Holmquist TJ (1988) J Appl Phys 64:3901
38. Imayev VM, Imayev RM, Salishchev GA, Povarova KB, Shagiev MR, Kuznetsov AV (1997) Scr Mater 36:891
39. Gray GT III (1994) In: Yoo MH, Wuttig M (eds) Twinning in advanced materials. The Minerals, Metals & Materials Society, Warrendale
40. Reed-Hill R, Abbaschian R (1992) Physical metallurgy principles. PWS-Kent, Boston, MA
41. Meyers MA, Vohringer O, Lubarda VA (2001) Acta Mater 49:4025
42. Meyers MA (1994) Dynamic behavior of materials. Wiley, New York